SMGroup

SM Analytical and Bioanalytical Techniques

Research Article

Cramer Rao Lower Bound CRB Shape Detection Method

Ahmad T Abdulsadda*

Department of Aerodynamic, Al Fuarat Al Awast University, Iraq

Article Information

Received date: May 11, 2017
Accepted date: Jul 24, 2017
Published date: Jul 31, 2017

***Corresponding author**

Ahmad T Abdulsadda, Department of Aerodynamic, Al Najaf Technical Institute, Al Fuarat Al Awast University, Al Najaf, Iraq, Email: ahmadabdulsadda@yahoo.com

Abstract

In this paper we investigate the problem of tracking a moving but non-vibrating cylindrical object and estimating its size and shape using an artificial lateral line system, an d determine the lower bound that the estimator can be reached. Based on a nonlinear analytical model for the moving object-induced flow field, a two-stage extended Kalman filter is proposed to estimate the location, velocity, size, and shapes of the object. Simulation results on tracking an ellipsoidal cross-section are presented to illustrate the approach.

Introduction

An engineering equivalent of a biological lateral line is of great interest to the navigation and control of underwater robots and vehicles. In particular, an artificial lateral line will represent a new, noiseless sensing modality for underwater applications that is complementary to traditional sensors such as vision and sonar [1,2].

The horizontal line framework (Artificial Lateral Line ALL) is a vital tangible organ for fish and oceanic creatures of land and water [1,3], and it is included in different creature practices, including prey/predator location [4], tutoring [5], rheotaxis [6], romance and correspondence [3]. A horizontal line comprises of varieties of supposed neuromasts, each containing packs of tactile hairs, epitomized in a thick structure called cupola. Under an impinging stream, the hairs are diverted, which evokes terminating of the hair cell neurons and hence empowers the creature to distinguish close field objects of intrigue and perform hydrodynamic imaging of the earth.

It is important to create simulated parallel line frameworks for submerged applications. This would give another detecting module in supplement to existing detecting components, for example, sonar and imaging, and encourage the control and coordination of submerged robots and vehicles. Building of sidelong line sensors has gotten expanding enthusiasm for as far back as couple of years. On the equipment side, varieties of stream sensors, unequivocally propelled by the organic sidelong line, have been created in light of different transduction standards, for example, hot wire anemometry [7], piezoresistivity [8], capacitive detecting [9], and typified interface bilayers [10]. We have as of late revealed a simulated horizontal line that endeavors the detecting capacity of Ionic Polymer-Metal Composite (IPMC) materials [11].

There have additionally been various flag preparing plans proposed for simulated ALL lines. The majority of these plans have been centered around the issue of restricting a vibrating circle, known as a dipole. Dipole sources have been widely utilized as a part of physiological and behavioral investigations of natural parallel lines, since they give basic copying of tail beating or member development of amphibian creatures. What's more, logical articulations of the subsequent stream field under a dipole are accessible, which encourages the calculation improvement. Revealed flag preparing plans have included misuse of the trademark focuses (e.g., zero-intersections, maxima, and so on.) in the deliberate speed profile [9], coordinating of the deliberate information with pre-gotten formats [12], beam forming procedures [8], and counterfeit neural systems [11]. Most existing work manages a dipole source that has settled vibration sufficiency and introduction. At the point when the vibration abundance is fluctuating, the issue winds up noticeably difficult, mostly on the grounds that a source far away yet with extensive vibration and another source adjacent yet with little vibration could deliver signs of comparative amplitudes. Such uncertainty is tended to by our current work [13], where a nonlinear estimation issue is planned in light of a diagnostic model of the dipole-created stream field. There the source area and the vibration plenty fullness are dealt with as questions that we try to recognize, given the stream adequacy estimation by the sensor exhibit.

In this paper we extend the work in [13] to consider the estimation and derive the mathematical statistical CBR to the moving but not vibrating object and estimate its shape parameters. If we consider the scenario of one fish detecting a predator using its lateral line system , the solution to the aforementioned problem would imply that the fish not only knows where the predator is, but also which way it is swimming toward. There are similar implications for artificial later al line systems.

To solve this problem, we treat the source location, it velocity and shape parameters as unknowns of a nonlinear estimation problem, and then present non linear Kalman filtering method.

Simulation results have been conducted to examine the effectiveness of the proposed scheme. Simulation has been conducted to examine the effectiveness of the proposed scheme. The remainder of this paper is organized as follows. We first present the model for the flow field generated by a moving object in a two-dimensional (2D) potential flow, and formulate the estimation problem in Section II. The filtering scheme is described in Section III, followed by the simulation CBR analysis in Section IV. Finally concluding remarks are provided in Section V.

Flow Model and Problem Formulation

In this paper we accept a two-dimensional (2D) potential stream. Consider a barrel shaped protest traveling through a generally still liquid. We initially introduce the unique instance of roundabout cross-area, and afterward sum up the model to a subjective cross-segment profile utilizing the conformal mapping hypothesis.

Consider the 2D plane $z = x + iy$. Without the loss of generality, assume that the cylinder is moving along x-direction with its cross-section lying in the x - y plane. The complex potential $w^c(z)$, where z is outside the region occupied by the cylinder, is given by [14].

$$w^c(z) = vx\frac{R^2}{z\text{-}z_1}, \tag{1}$$

Where the superscript c indicates the case of a circular profile, v_x denotes the moving speed, R is a radius of the circular cross-section, and $z_1 = xs + iy_s$ denotes the center of the moving cylinder. The corresponding complex flow velocity W^c is then given by

$$w^c(z) = \frac{dw^c(z)}{dz} = -vx\frac{R^2}{(z\text{-}z_1)^2}. \tag{2}$$

If we write $w^c(z) = v_x^c + i\, v_y^c$, then

$$v_x^c = -\frac{v_x R^2((x\text{-}x_s)^2 - (y\text{-}y_s)^2)}{((x\text{-}x_s)^2 + (y\text{-}y_s)^2)^2}, \tag{3}$$

$$v_y^c = \frac{2v_x R^2 (y\text{-}y_s)^2 - (x\text{-}x_s)}{((x\text{-}x_s)^2 + (y\text{-}y_s)^2)^2}. \tag{4}$$

For a cylinder with a general shape (Figure.1), its cross-section profile can be obtained by mapping the circular profile with the Laurent series expansion [15]:

$$\zeta(z) = (z\text{-}z_1) + \frac{\lambda_1}{(z\text{-}z_1)} + \frac{\lambda_2}{(z\text{-}z_1)^2} + \ldots\ldots, \tag{5}$$

Where $\lambda_1, \lambda_2, \cdots$, are the shape parameters. When the shape parameters are real, the obtained shape will be symmetric with respect to the *x*-direction. It can be shown that the complex flow velocity $W^g(z)$ around the moving object with a general profile is

$$W^g(z) = \frac{dw^c(z)}{dz}\frac{dz}{d\zeta} = \frac{v_x\left(-\frac{R^2}{(z\text{-}z_1)^2}\right)\left(1 - \frac{\lambda_1}{(z\text{-}z_1)^2} - \frac{2\lambda_2}{(z\text{-}z_1)^3} - \ldots\right)^{-1}}{W^c(z)\,\frac{dz}{d\zeta}}. \tag{6}$$

In (6), z ∈ D, the domain exterior to the object with the general profile. Since the impact of higher-order

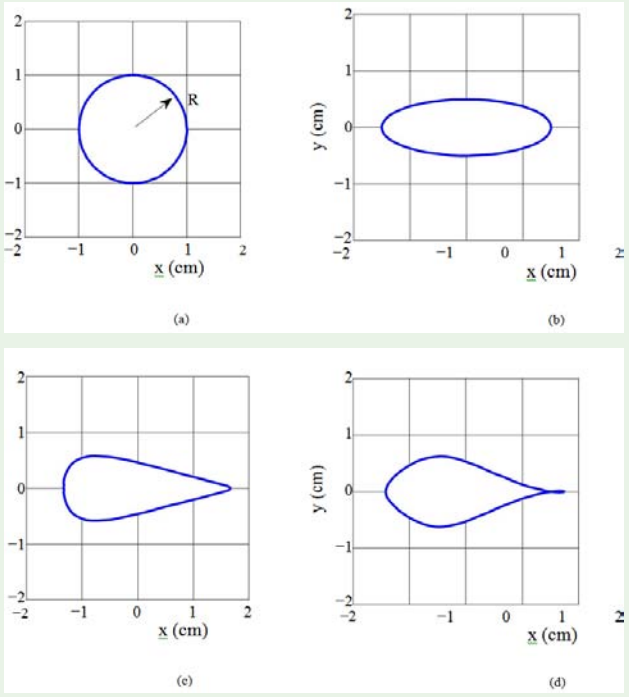

Figure 1: Illustration of the Laurent series expansion : (a) Circle $\zeta(z) = z$; (b) the shape fingerprint $\zeta(z) = z + 1/(2z)$; (c) the shape fingerprint $\zeta(z) = z + 1/(2z) + 1/(6z^2)$; (d) the shape fingerprint $\zeta(z) = z + 1/(2z) + 1/(6z^2) + 1/(12z^3)$ (adapted from [15]).

Terms in (5) decays quickly with the distance from the object [15], in this chapter, we consider the case of ellipsoidal profile only, namely, $\lambda_1 \neq 0, \lambda_i = 0, \forall_i > 1$. Furthermore, we assume that λ_1 is real. Using (6), we can derive the complex flow velocity $W^e(z)$ around an ellipsoidal cylinder:

$$W^e(z) = v_x\left(-\frac{R^2}{(z\text{-}z_1)^2}\right)\left(1 - \frac{\lambda_1}{(z\text{-}z_1)^2} - \frac{2\lambda_2}{(z\text{-}z_1)^3}\right)^{-1}. \tag{7}$$

If we write $W^e(z) = v_x^e + i\, v_y^e$, then

$$v_x^e = -\frac{v_x R^2\left((x\text{-}x_s)^2 - (y\text{-}y_s)^2 - \lambda_1 - 2\lambda_2\right)}{((x\text{-}x_s)^2 - (y\text{-}y_s)^2 - \lambda_1 - 2\lambda_2)^2 + 4(x\text{-}x_s)^2(y\text{-}y_s)^2}, \tag{8}$$

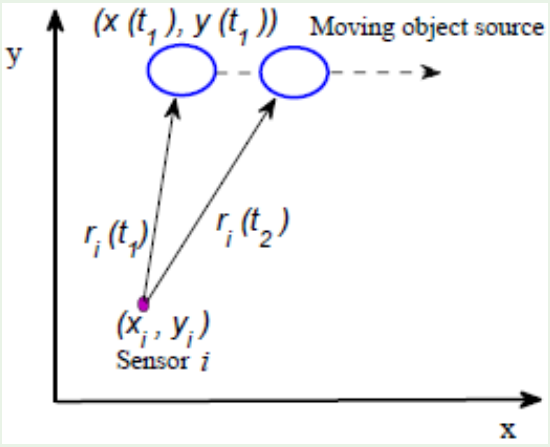

Figure 2: Illustration of the problem setup for the tracking and estimation of a moving object.

$$v_y^e = -\frac{2v_x R^2 (y-y_s)(x-x_s)}{((x-x_s)^2-(y-y_s)^2-\lambda_1-2\lambda_2)^2+4(x-x_s)^2(y-y_s)^2}. \quad (9)$$

We now formulate the problem of localizing a moving object with ellipsoidal profile and estimating its size/shape in the x-y plane using an array of flow sensors. Consider Figure 2, where an artificial lateral line comprising N sensors is located in parallel to the x-axis, with the sensor locations denoted as $(x_i, y_i), 0 \le i \le N-1$. We denote the center of the moving cylinder at time t by $(x_s(t), y_s(t))$. The object is assumed to move with a constant speed V_x parallel to the lateral line. We further assume that the presence of sensors has negligible effect on the flow field generated by the moving object. Each sensor is assumed

to provide a noisy measurement of the local flow velocity V_x along the x-direction. In particular, the measurement $m_i(t)$ by sensor *i* at time *t* is given by

$$m_i(t) = f^e(x_i, y_i, x_s(t), y_s(t), v_x, R, \lambda 1, \lambda 2) + n_i(t), \quad (10)$$

Where the function f^e follows from (8), and n_i is the measurement noise. We introduce a compact notation for the measurements from all sensors,

$$M(t) = [m_1(t) \cdots m_N(t)]^T = F^e(x_s(t), y_s(t), v_x, R, \lambda_1, \lambda_2) + n(t),$$

Where ^{T} denotes transpose,

$$F^e(x_s, y_s, v_x, R, \lambda_1, \lambda_2) \triangleq [f^e(x_1, y_1, x_s, y_s, v_x, R, \lambda_1, \lambda_2) \ldots f^e(x_N, y_N, x_s, y_s, v_x, R, \lambda_1, \lambda_2)]^T,$$

and $n(t) = [n_1(t) \ldots n_N(t)]^T$.

The estimation problem is then formulated as: given the measurements from the artificial lateral line, $M(\cdot)$, determine the object location $(x_s(t), y_s(t))$, speed V_x, size parameter R, and shape parameters λ_1, λ_2.

Extended Kalman Filter

In this paper we propose to solve the tracking and estimation problem with extended Kalman filtering. We first provide a brief review of extended Kalman filtering, when the measurement equation involves nonlinearities [16]. The discrete-time setting is considered in this work, where the time index is denoted by *k*. Suppose that the system dynamics is given by

$$X_k = A_{k-1} X_{k-1} + w_{k-1},$$
$$M_k = f(X_k) + n_k. \quad (11)$$

Where $X_k \in \mathbb{R}^n$ denotes the state vector, A_{k-1} has dimensions $n \times n$, $M_k \in \mathbb{R}^p$ denotes the measurement, $f(\cdot)$ is a nonlinear function, and $w_{k-1} \in \mathbb{R}^n$ and $d_k \in \mathbb{R}^p$ denote the process noise and the measurement noise, respectively. It is assumed that W_{k-1} and n_k are white, zero-mean, Gaussian noises, with covariance matrices denoted as Q_k and C_k, respectively. It is also assumed that W_{k-1} and n_k are uncorrelated with each other.

Since $f(X_k)$ is a nonlinear function, in extended Kalman filtering, it is linearized at $\hat{X}_{k|k-1}$, the prediction for X_k at time $k-1$. In particular, $f(X_k)$ is approximated by

$$f(X_k) \approx f(\hat{X}_{k|k-1}) + \hat{H}_k (X_k - \hat{X}_{k|k-1}), \quad (12)$$

where $\hat{H}_K$ is the Jacobin matrix of $f(\cdot)$ evaluated at $\hat{X}_{k|k-1}$:

$$\hat{H}_k = \left.\frac{\partial f(X_k)}{\partial X_k}\right|_{X_{k=\bar{X}_{k|k-1}}}. \quad (13)$$

At $k = 0$, the initial state estimate $\hat{X}_{0|0} = X_0$ is a random vector with known mean $\mu_0 = E[X_0]$, and the initial covariance matrix is given by $P_{0|0} = E\left[(X_0 - \mu_0)(X_0 - \mu_0)^T\right]$. The main steps in an extended Kalman filter are outlined next. The state prediction is given by

$$\hat{X}_{k|k-1} = A_{k-1} \hat{X}_{k-1|k-1}. \quad (14)$$

For $k \ge 1$, the prediction of state covariance matrix follows

$$P_{k|k-1} = A_{k-1} P_{k-1|k-1} A_{k-1}^T + Q_{k-1}, \quad (15)$$

and the optimal gain matrix K_k is given by

$$K_k = P_{k|k} \hat{H}_k^T (C_k + \hat{H} P_{k|k-1} \hat{H}_K^T)^{-1} \quad (16)$$

Finally, the estimates of the state and its covariance matrix are updated via

$$\hat{X}_{k|K} = X_{k|K-1} + K_k (M_k - f(\hat{X}_{k|k-1})) \quad (17)$$

$$P_{k|k} = (I - K_k \hat{H}_k) P_{k|k-1} \quad (18)$$

where *I* denotes the identity matrix.

For our tracking and estimation problem, the dynamics of interest can be described as follows:

$$x_s[k] = x_s[k-1] + v_x[k-1]\Delta + w_1[k-1], \quad (19)$$

$$y_s[k] = y_s[k-1] + v_y[k-1]\Delta + w_2[k-1], \quad (20)$$

$$v_x[k] = vx[k-1] + w_3[k-1], \quad (21)$$

$$v_y[k] = v_y[k-1] + w_4[k-1], \quad (22)$$

$$R[k] = R[k-1] + w_5[k-1], \quad (23)$$

$$\lambda 1[k] = \lambda 1[k-1] + w_6[k-1], \quad (24)$$

$$\lambda 2[k] = \lambda 2[k-1] + w_7[k-1], \quad (25)$$

(26)

where Δ is the sampling time, and $w_1, \cdots w_7$ denote the process noises, which are assumed to be uncorrelated. The measurement equation is given by

$$M[k] = F^e(x_s[k], y_s[k], v_x[k], R[k], \lambda_1[k], \lambda_2[k]) + n_{[k]}, \quad (27)$$

where n[*k*] denotes the vector of measurement noises with uncorrelated components.

In this work, we propose a multiple-stage nonlinear filtering scheme, as illustrated in Figure. 3. In the first stage, five state components, (19) - (23), are estimated while assuming the shape parameters $\lambda_{1=0}, \lambda_{2=0}$. Correspondingly, the measurement equation for the first stage is obtained by plugging $\lambda_{1=0}$ and $\lambda_{2=0}$ (27):

$$M[k] = F^e(x_s[k], y_s[k], v_x[k], R[k], 0, 0) + n[k]. \quad (28)$$

In the second stage, the state estimate involves λ_1 and λ_2 (equation (24)), while the measurement equation is obtained from (27) by plugging in the state estimates from the first stage:

$$M[k] = F^e(\hat{x}_{s,k|k}, \hat{y}_{s,k|k}, \hat{v}_{x,k|k}, \hat{R}_{k|k}, \lambda_1, \lambda_2) + n[k]. \quad (29)$$

State estimation at each stage is then carried out following the general nonlinear filtering procedure, as outlined earlier.

There are two motivations for estimating the desired information in two cascaded stages. First, as discussed in [15], it is likely that a biological lateral line extracts the relevant information in a progressive manner. Second, the proposed scheme leads to reduced computational complexity because of the reduced dimensions for the state dynamics - for example, one only needs to invert 6 × 6 matrices instead of 7 × 7 matrices.

Simulation Results

Recursive information matrix

Generally, a nonlinear filtering problem does not have a close-form analytical solution, and in all practical applications, nonlinear filtering is performed b y some sort of approximation. Despite the absence of a closed-form solution, we would like to find the best achievable error performance for nonlinear filtering; to do so, a theoretical Cramer-Rao lower bound has been formulated for such problems. Consider the system which is described in (11), the recursive information matrix J_k for such system has been derived in [16] as

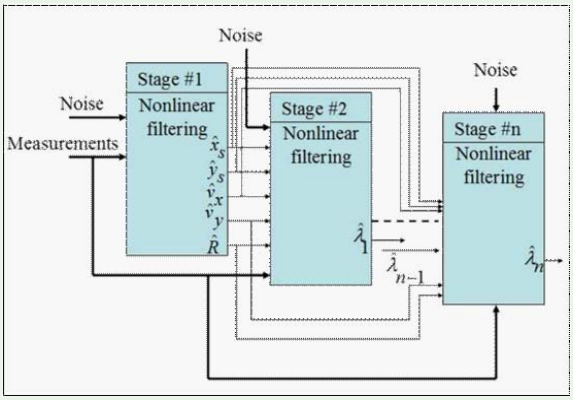

Figure 3: Illustration of the n-stages filtering scheme.

$$J_k = Q_{k-1}^{-1} + \tilde{H}_k^T C_k^{-1} \tilde{H}_k - Q_{k-1}^{-1} A_{k-1} \left(J_{k-1} + A_{k-1}^T Q_{k-1}^{-1} A_{k-1} \right)^{-1} A_{k-1}^T Q_{k-1}^{-1} A_{k-1}, \quad (30)$$

where

$$\tilde{H} = \frac{\partial f(X_k)}{\partial X_k}. \quad (31)$$

is the Jacobian of $f(\cdot)$ evaluated at the true value of x_k.

Figure 4 shows the square root of the CRB, $\sqrt{CRB}$, corresponding to the components of the state vector: (i) x_s-coordinate, (ii) y_s-coordinate, (iii) size parameter R and (iv) shape parameter λ_1, for two-stage and one-stage schemes, respectively. These bounds are obtained as:

$$CRB(X_k[i]) = J^{-1}[i, i], \; i = 1,2,3,4. \qquad (32)$$

It is clear from Figure. 4 that, a two-stage scheme yields smaller estimation errors than a one-stage scheme. Consequently, we will employ two-stage schemes in our estimation, the analytical derivation steps of the CBR is described in appendix A.

Simulation results on nonlinear filtering

Figure 5 illustrates the simulation setup. The lateral line system is placed parallel to the x-axis and centered at (10, 0) cm. It consists of 12 sensors, with the sensor-to-sensor separation of 2 cm. The ellipsoidal cylinder, with a shape parameter $(\lambda_2 = \lambda_1 = 1.5\,\text{cm})$ and a size parameter R = 2.5 cm, moves from left to right with a constant speed of 6 cm/s. The initial location of the moving object is (0, 7) cm, and the time duration for the movement is 1.667 s, resulting in a terminal location of (20, 7) cm. The initial state estimates are

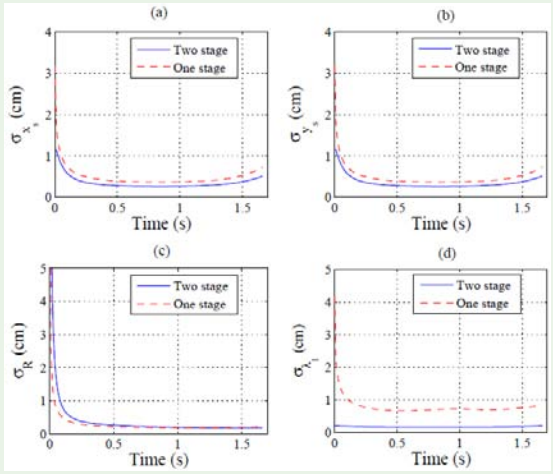

Figure 4: $\sqrt{CRB}$ for: (a) Moving object x_s coordinate; (b) moving object y_s coordinate; (c) size parameter R; (d) shape parameter λ_1.

Table 1: simulation results: estimated velocity, size parameter, and shape parameter under different process noise variances. Two-stage extended kalman filtering is used.

Parameter	Actual	Estimated (σ^2 = 0.1)	(σ^2 = 0.3)	(σ^2 = 0.5)
Velocity (cm/s)	6	6.22	6.35	6.44
Size R (cm)	2.5	2.34	2.41	2.32
Shape λ_1	1.5	1.23	1.42	1.43
Shape $\lambda_{2(cm)}$	1.5	1.26	1.46	1.45

set to be $\hat{x}_{s,0|0} = 0.1$ cm, $\hat{y}_{s,0|0} = 5$ cm, $\hat{v}_{x,0|0} = 4$ cm/s, $\hat{v}_{y,0|0} = 1$ cm/s, $R_{0|0} = 1$ cm, and $\lambda_{1,0|0} = 0.1$ cm. The sampling time D is chosen to be 0.01 s. Figure. 6 shows the simulated measurements of flow velocities (x-component) at all sensor sites, where a zero-mean, Gaussian noise with a variance of $(\sigma_m^2 = 0.01\text{cm}^2/\text{s}^2)$ is added to each measurement.

It can be observed that the estimated object location quickly converges to the neighborhood of the actual location after a short transient period (less than 0.15 s). In addition, while the variance of the process noises does influence the transients, its impact on t he estimation performance at the steady state is not pronounced. The insensitivity of the estimation performance to the process noise variances is positive news, since it is difficult to precisely characterize

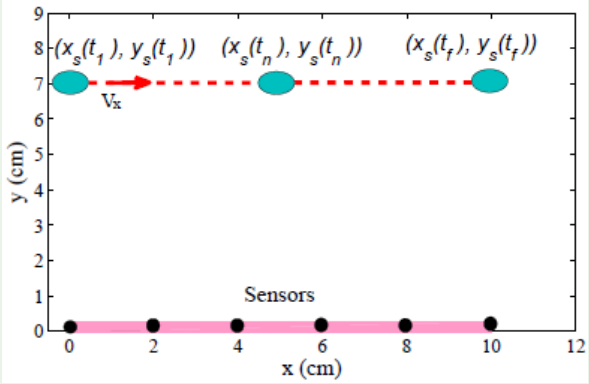

Figure 5: Simulation setup for tracking of a moving cylinder.

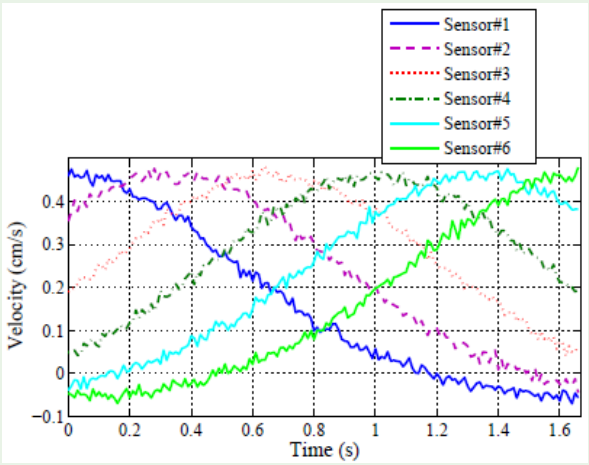

Figure 6: Simulated time trajectories of sensor measurements.

these noise variance values in practice. Table I summarizes the averages of the estimates for other parameters $(v_x, R \text{ and } \lambda_1)$, where each average is obtained by taking the mean of the estimated values over the period [0.33, 1.67] s.

Conclusion

We investigate the problem of tracking a moving but non-vibrating cylindrical object and estimating its size and shape using an artificial lateral line system. Instead of using pressure sensing as done in the literature for similar problems [15,17,18], we consider the measurement of flow velocities as is believed to be what is adopted in biological lateral lines. Based on a nonlinear analytical

model for the moving object-induced flow field, two-stage nonlinear filtering algorithms are proposed to estimate the location, velocity, size, and shape of the object. Using two-stage filtering instead of one stage is motivated partly by the progressive information extraction conjectured for biological lateral lines [15], and partly by computational efficiency. The approach is illustrated with simulation results, where a moving object is tracked and its shape parameter estimated.

In future work, we will try to verify the simulation results by doing experimental setup, where an artificial lateral line consisting of 12 nano smart IPMC sensors will design and implement as prototype to track and estimate the size and the shape of robot like fish.

Appendix (A)

Based on the measurement equation (11), the likelihood function is given by

$$p(M;X)=\frac{1}{2\pi\sigma_m^2}e\left(\frac{-1}{2\pi\sigma_m^2}\Sigma_{i=0}^{N-1}\left(M_i-f_i(X)\right)^2\right) \quad (33)$$

Differentiating the log of the likelihood function twice, we get:-

$$\frac{\partial^2}{\partial^2 X}1n(p(M;X))=\frac{1}{\sigma_m^2}\sum_{i=0}^{N-1}\left\{(M_i-f_i(X))\frac{\partial^2 f_i(X)}{\partial^2 X}-\left[\frac{\partial f_i(X)}{\partial X}\right]\left[\frac{\partial f_i(X)}{\partial X}\right]^T\right\} \quad (34)$$

The Fisher information matrix is defined by $-E\left[\frac{\partial^2(1np(M;X))}{(\partial X)^2}\right]$, which is given by

$$F=\frac{1}{\sigma_m^2}\sum_{i=0}^{N-1}\left[\frac{\partial f_i(X)}{\partial X}\right]\left[\frac{\partial f_i(X)}{\partial X}\right]^T$$

Where $E[\cdot]$ is the expectation taken over all possible measurement M. the i^{th} diagonal of the inverse of F, which is denoted by $F_{i,i}^{-1}$, provides a lower bound on the variance of the i^{th} element of the state estimate $\hat{X}$. Generally, $Var(\hat{X})\geq F_{i,i}^{-1}$.In our case we have four elements and F is just a 4×4 matrix. The Fisher information matrix can be expressed as $F=[F_{11},F_{12},F_{12}^T,F_{22}]$, where the sub-matrix blocks F_{11}, F_{12}, and F_{22} are 2×2 matrices,

$$F_{11}=\frac{1}{\sigma_m^2}\begin{bmatrix}\Sigma_{I=1}^N\left(\frac{\partial f_i(\cdot)}{\partial x_s}\right)^2 & \Sigma_{i=1}^N\left(\frac{\partial f_i(\cdot)}{\partial x_s}\right)\left(\frac{\partial f_i(\cdot)}{\partial y_s}\right)\\ \Sigma_{I=1}^N\left(\frac{\partial f_i(\cdot)}{y_s}\right)\left(\frac{\partial f_i(\cdot)}{x_s}\right) & \Sigma_{i=1}^N\left(\frac{\partial f_i(\cdot)}{y_s}\right)^2\end{bmatrix},$$

$$F_{12}=\frac{1}{\sigma_m^2}\begin{bmatrix}\Sigma_{I=1}^N\left(\frac{\partial f_i(\bullet)}{\partial x_s}\right)\left(\frac{\partial f_i(\cdot)}{\partial R}\right) & \Sigma_{I=1}^N\left(\frac{\partial f_i(\cdot)}{\partial x_s}\right)\left(\frac{\partial f_i(\cdot)}{\partial \lambda_1}\right)\\ \Sigma_{I=1}^N\left(\frac{\partial f_i(\cdot)}{y_s}\right)\left(\frac{\partial f_i(\cdot)}{\partial R}\right) & \Sigma_{I=1}^N\left(\frac{\partial f_i(\bullet)}{\partial y_s}\right)\left(\frac{\partial f_i(\cdot)}{\partial \lambda_1}\right)\end{bmatrix},$$

$$F_{22}=\frac{1}{\sigma_m^2}\begin{bmatrix}\Sigma_{I=1}^N\left(\frac{\partial f_i(\cdot)}{\partial R}\right)^2 & \Sigma_{i=1}^N\left(\frac{\partial f_i(\cdot)}{\partial R}\right)\left(\frac{\partial f_i(\cdot)}{\partial \lambda_1}\right)\\ \Sigma_{I=1}^N\left(\frac{\partial f_i(\cdot)}{\partial \lambda_1}\right)\left(\frac{\partial f_i(\cdot)}{\partial R}\right) & \Sigma_{i=1}^N\left(\frac{\partial f_i(\cdot)}{\partial \lambda_1}\right)^2\end{bmatrix},$$

Where

$$\frac{\partial f(\cdot)}{\partial x_s}=v_x R^2\left\{\frac{2(x-x_s)}{\left((x-x_s)^2-(y-y_s)^2-\lambda_1\right)^2+4(x-x_s)^2(y-y_s)^2}-\frac{4(x-x_s)\left((x-x_s)^2-(y-y_s)^2-\lambda_1\right)\left((x-x_s)^2+(y-y_s)^2-\lambda_1\right)}{\left(\left((x-x_s)^2-(y-y_s)^2-\lambda_1\right)^2+4(x-x_s)^2(y-y_s)^2\right)^2}\right\}$$

$$\frac{\partial f(\cdot)}{\partial y_s}=v_x R^2\left\{\frac{-2(y-y_s)}{\left((x-x_s)^2-(y-y_s)^2-\lambda_1\right)^2+4(x-x_s)^2(y-y_s)^2}-\frac{4(y-y_s)\left((x-x_s)^2-(y-y_s)^2-\lambda_1\right)\left(-(x-x_s)^2(y-y_s)^2-\lambda_1\right)}{\left(\left((x-x_s)^2-(y-y_s)^2-\lambda_1\right)^2+4(x-x_s)^2(y-y_s)^2\right)^2}\right\}$$

$$\frac{\partial f(\cdot)}{\partial R}=-2v_x R\left\{\frac{\left((x-x_s)^2-(y-y_s)^2-\lambda_1\right)}{\left((x-x_s)^2-(y-y_s)^2-\lambda_1\right)^2+4(x-x_s)^2-(y-y_s)^2}\right\},$$

$$\frac{\partial f(\cdot)}{\partial \lambda_1}=v_x R^2\left\{\frac{1}{\left((x-x_s)^2-(y-y_s)^2-\lambda_1\right)^2+4(x-x_s)^2-(y-y_s)^2}-\frac{2\left((x-x_s)^2-(y-y_s)^2-\lambda_1\right)^2}{\left((x-x_s)^2-(y-y_s)^2-\lambda_1\right)^2+4(x-x_s)^2-(y-y_s)^2}\right\}$$

and the Cramer-Rao bound is defined as F^{-1}, where F^{-1} is given by

$$F^{-1}=\begin{bmatrix}J^{-1} & -JF_{12}F_{22}^{-1}\\ F_{22}^{-1}F_{21}J^{-1} & F_{22}^{-1}\left(I+F_{21}J^{-1}F_{12}\right)\end{bmatrix},$$

where $J=F_{11}-F_{12}F_{22}^{-1}F_{21}$. J is a 2×2 matrix given by

$$J=\begin{bmatrix}J_{1,1} & J_{1,2}\\ J_{2,1} & J_{2,2}\end{bmatrix},$$

The CRBs for the estimates of x_s and y_s are given by $J_{1,1}^{-1}=|J|^{-1}.J^{2,2}$ and $J_{2,2}^{-1}=|J|^{-1}.J_{1,1}$ respectively.

Specifically,

$$CRB(x_s)=J_{1,1}^{-1},CRB(y_s)=J_{2,2}^{-1}. \quad (35)$$

Acknowledgement

The author would like to thank professor Xiabo Tan, manger of Smart Micorsystem Lab. , Michigan State University (MSU), for guiding the author where this work can be considered as one direction of proposed future work of Abdulsadda PHD. Thesis.

References

1. Coombs S. Smart skins: Information processing by lateral line flow sensors. Autonomous Robots. 2001; 11: 255–261.

2. Liu C. Micromachined biomimetic artificial haircell sensors. Bioinsp Biomim. 2007; 2: S162-S169.

3. Coombs S, Braun CB. Information processing by the lateral line system. in Sensory Processing in Aquatic Environments, SP Collin and NJ Marshall, Eds. New York: Springer-Verlag. 2003; 122-138.

4. Pohlmann K, Atema J, Breithaupt T. The importance of the late ral line in nocturnal predation of piscivorous catfish. J Exp Biol. 2004; 207: 2971-2978.

5. Pitcher TJ, Partridge BL, Wardle CS. A blind fish can school. Science. 1976; 194: 963-965.

6. Gardiner JM, Atema J. Sharks need the lateral line to locate or sources: Rheotaxis and eddy chemotaxis. J Exp Biol. 2007; 210: 1925-1934.

7. Yang Y, Chen J, Engel J, Pandya S, Chen N, Tucker C, et al. Distant touch hydrodynamic imaging with an artificial lateral line. Proceedings of the National Academy of Sciences. 2006; 103: 18891-18895.

8. Yang Y, Nguyen N, Chen N, Lockwood M, Tucker C, et al. Artificial lateral line with biomimetic neuromasts to emulate fish sensing. Bioinsp. Biomim. 2010; 5: 016001.

9. Dagamseh AMK, Lammerink TSJ, Kolster ML, Bruinink CM, Wiegerink RJ, Krijnen GJM. Dipole-source localization using biomimetic flow-sensor arrays positioned as lateral-line system. Sensors and Actuators A. Physical. 2010; 162: 355-360.

10. Sarles SA, Pinto P, Leo DJ. Hair cell sensing with encapsulated interface bi layers. in Proceedings of Bioinspiration, Biomimetics, and Bioreplication, ser. Proceedings of SPIE. 2011; 7975: 797509.

11. Abdulsadda AT, Tan X. Underwater source localization using an IPMC-based artificial lateral line. in Proceedings of the 2011 IEEE International Conference on Robotics and Automation, Shanghai, China. 2011; 447–452.

12. Pandya S, Yang Y, Jones DL, Engel J, Liu C. Multisensor processing algorithms for underwater dipole localization and tracking using MEMS artificial lateral-line sensors. EURASIP Journal on Applied Signal Processing. 2006; 2006: 8.

13. Abdulsadda AT, Zhang F, Tan X. Localization of source with unknown amplitude using IPMC sensor arrays. in Proceedings of Electro active Polymer Actuators and Devices (EAPAD) XIII, ser. Proceedings of SPIE, Y. Bar-Cohen, Ed. 2011; 7976: 797627.

14. P RL, Incompressible flow. New York: Wiley, 1985.

15. Bouffanais R, Weymouth GD, Yue DKP. Hydrodynamic object recognition using pressure sensing. Proc. R. Soc. A. 2011; 467: 19-38.

16. B. Ristic, S. Arulampalam, and N. Gordon. Beyond the Kalman Filter. London: Artech House. 2004.

17. Fernandez VI, Maertens A, Yaul FM, Dahl J, Lang JH, Triantafyllou MS, et al. Lateral-line-inspired sensor arrays for navigation and object identification. Mar Technol Soc J. 2011; 45: 130-146.

18. Venturelli R, Akanyeti O, Visentin F, Ježov J, Chambers LD, Toming G. Chambers, et al. Hydrodynamic pressure sensing with an artificial lateral line in steady an d unsteady flows. Bioinspir Biomim. 2012; 7: 036004.